Research Square

Preprints are preliminary reports that have not undergone peer review.
They should not be considered conclusive, used to inform clinical practice,
or referenced by the media as validated information.

Novel 3D porous TMU-12 metal–organic framework based on cobalt clusters, a promising material for fabricating flexible supercapacitor electrodes

Hamideh Mohammadian-Sarcheshmeh
Yazd University
Mohammad Mazloum-Ardakani
mazloum@yazd.ac.ir
Yazd University
Meysam Safari
Yazd University

Article

Keywords: Cobalt, Flexible electrode, Novel MOF, Supercapacitor, TMU-12

Posted Date: August 28th, 2026

DOI: https://doi.org/10.21203/rs.3.rs-10313701/v1

License: This work is licensed under a Creative Commons Attribution 4.0 International License.
Read Full License

Additional Declarations: No competing interests reported.

Abstract

Supercapacitors are promising energy storage devices due to their high power density, long cycle life, and structural simplicity. Metal–organic frameworks (MOFs) are attractive electrode materials, offering three-dimensional porous structures, high surface area, chemical tunability, ionic permeability, and thermal stability, making them suitable for flexible electronics. In this work, for the first time, a previously reported cobalt-based MOF, TMU-12 (TMU: Tarbiat Modares University), is introduced as an active material for flexible supercapacitor electrodes. The TMU-12 MOF, synthesized via a solvothermal method using $Co(NO_3)_2 \cdot 6H_2O$, 4,4'-oxibisbenzoic acid (H_2oba), and pyrazine, is employed without any modification. The fabricated TMU-12/CF electrode delivers a specific capacitance of 206.93 $F \cdot g^{-1}$ at 0.005 $V \cdot s^{-1}$ in 3.0 M KOH, with outstanding capacitance retention of 90.85% after 2000 cycles, demonstrating excellent electrochemical stability. Notably, compared with other cobalt-based MOF electrodes, TMU-12/CF offers competitive capacitance while exhibiting significantly superior cycling stability, ranking among the most stable cobalt-MOF systems reported. This remarkable combination of high performance, exceptional durability, and flexibility highlights TMU-12 as a promising candidate for next-generation flexible supercapacitors, paving the way for utilizing existing MOFs in advanced energy storage applications.

1. Introduction

The growing global population, depletion of fossil fuels, and global warming resulting from greenhouse gas emissions have significantly increased the demand for sustainable energy sources, such as wind, hydrogen, and solar energy. Unfortunately, these sources of energy are not always available and are completely affected by natural conditions [1, 2]. Consequently, energy storage systems, including supercapacitors and batteries, can significantly impact sustainable energy sources and attract considerable attention [3–6]. Compared to other storage systems, supercapacitors have presented remarkable potential for energy storage technology due to their remarkable properties, including high power capability, high energy density, structural simplicity, and long-term durability [7, 8]. Supercapacitors fill the energy gap between batteries and conventional electrochemical capacitors. They have been utilized in various fields, including electronic communication, electric transportation, and aerospace, due to their effective performance in energy storage. Although they have been theoretically recognized as a source of acceptable energy storage systems and have been utilized in various applications, their performance still needs to be further improved to address the ever-increasing energy needs of modern societies [9]. The materials used to make the electrodes in supercapacitors have a significant impact on their electrochemical performance. Metal-organic frameworks (MOFs) are a group of practical compounds with outstanding features, including controllable morphology, adjustable chemical composition, and high porosity, which are known as acceptable precursors for the fabrication of porous nanostructure materials [10–12]. Compared to porous materials, such as metal complex hydrides, zeolites, and activated carbon, MOFs are known for their advantages, including simple synthesis, high temperature resistance, low density, a large internal surface area, and a distinct regular

structure. MOFs are practical suggestions for supercapacitor electrode materials due to their outstanding properties, including 3D porous architecture, structural tunability, large surface area, permeability to external elements, simple synthesis, and high temperature resistance[13–16]. Despite the successful developments in the fabrication of MOFs, controlling the morphological structure in MOF materials still presents challenges. To produce active materials with a high specific surface area acceptable for electrochemical applications, the development of MOF derivatives is important [17]. MOFs are known as organic-mineral hybrid materials that can be fabricated by selecting appropriate organic ligands and inorganic secondary building units. MOFs are synthesized by reinforcing bonds between transition metals and O/N with organic ligands [18, 19]. These organic ligands typically involve heteroatoms, such as P and N, and contain a significant amount of carbon. MOFs can be fabricated in different 1D, 2D, and 3D forms, depending on the structure of their organic and inorganic units used in their

synthesis [20]. In particular, compared to 1D and 2D MOF-based structures, 3D MOF structures exhibit several advantages, including a high surface area and a significant aspect ratio, i.e., a high surface-to-volume ratio. These features of 3D MOFs decrease the diffusion path of ions, thereby enhancing the specific capacity and rate capability of these types of MOF structures [21]. Because MOFs are designable and readily available for functionalization, they are highly practical for applications such as drug delivery, sensing, ion exchange, gas storage/separation, and catalysis [22, 23]. Additionally, MOFs are suitable candidates for achieving the improved electrochemical performances required in supercapacitors. As previously mentioned, MOFs have a large surface area, some tunable properties, abundant micropores, and variable sites for redox reactions, making them acceptable for various energy applications [24, 25]. The use of MOFs in the construction of supercapacitors is divided into three groups. Pristine MOFs are the first group that stores energy via reversible redox reactions at the metal centers or through the physical adsorption of electrolyte ions on their inner surfaces [26]. Electrodes based on MOF-derived metal oxides are known as the second group, which can store energy through charge transfer between the electrolyte ions and the electrode. The third group includes the use of MOF-derived porous carbons, which are created through the pyrolysis of the MOF template [26–28]. The different porous MOFs have been fabricated recently. Various methods, depending on the desired properties and the targeted final structures for MOFs, have been used to synthesize MOFs. These methods include microwave heating/ultrasound irradiation, hydrothermal/solvothermal, electrochemical, mechanochemical, and reaction-diffusion methods [29–37]. The hydrothermal method has been widely used. It is generally performed in the temperature range from 80 to 250°C. This method has garnered significant attention due to its capability for large-scale industrial production. Co8-MOF-5 was reported as the first pristine MOF to fabricate a supercapacitor electrode [38]. Due to its low electrical conductivity, this electrode showed a low specific capacitance. MIL-47, Co-MOF-71, and MIL-100(Fe) are other pristine MOFs utilized to fabricate supercapacitor electrodes [39–41].

In this research, a 3D porous cobalt-based metal–organic framework,

$[Co_3(oba)_3(O)\ (Py)_{0.5}]_n$·4DMF·Py (TMU-12) was fabricated using a simple solvothermal procedure by mixing $Co(NO_3)_2$·$6H_2O$, 4,4-Oxibis benzoic acid (H_2oba), and pyrazine [42, 43]. Different techniques, such as Field emission scanning electron microscopy (FESEM), FT-IR, energy-dispersive X-ray spectroscopy (EDX), and X-ray diffraction (XRD) analyses, were used to characterize the morphology and structure of the TMU-12 material.

In this study, a flexible supercapacitor electrode was fabricated for the first time using the TMU-12 compound. The flexible electrode was simply prepared using carbon felt (CF) as the substrate. The electrochemical behaviors of the introduced flexible electrode (TMU-12/CF) were examined using a potentiostat/galvanostat device (PGSTAT-302 N, Eco Chemie, Netherlands) through cyclic voltammetry (CV), galvanostatic charge/discharge (GCD), and electrochemical impedance spectroscopy (EIS). Some initial optimizations were examined. The TMU-12 /CF electrode indicated an acceptable C_{SP} value of 206.93 F. g^{-1} at = 0.005 $V.s^{-1}$. Moreover, the

TMU-12 /CF electrode exhibited a specific capacitance retention of 90.85% after recording 2000 cycles in the 3.0 M KOH electrolyte solution, demonstrating its significant stability. In this work, a symmetric supercapacitor device (two-electrode system) was prepared using the same electrode for the anode and cathode. For the designed supercapacitor, amounts of 7.93 Wh. kg^{-1} and

3.2 kW. Kg^{-1} were obtained for energy density (E) and power density (P), respectively.

2. Experimental section

2.1. Materials

Ferric chloride (97%), sodium chloride (99%), hydrochloric acid (37%), cobalt (II) nitrate trihydrate (99%), 4,4-Oxibis benzoic acid (H_2oba, 99%), N, N-dimethylformamide (DMF, 99.8%), methanol (98%), and ethanol (99%) were purchased from Merck Company (Darmstadt, Germany).

2.2. Synthesis of TMU-12

TMU-12 was synthesized by mixing pyrazine (0.5 mm), oba = 4,4′-oxybisbenzoic acid) (0.5 mm), and $Co(NO_3)_2.6H_2O$ (1 mm) in organic solvent (DMF 30 mL) in a Teflon-lined autoclave at 140 C for 48 h. The acquired powder was separated using centrifugation, washed with solvent several times, and dried [42].

2.3. Fabrication of the flexible supercapacitor electrode

The flexible supercapacitor electrode was assembled in a simple way. In order to fabricate the supercapacitor electrode, a slurry of synthesized TMU-12 was prepared by mixing electrode active material (90%) and PTFE (polytetrafluoroethylene) (10%) in ethanol, and then dispersing for 5 minutes.

The electrode substrate, carbon felt (CF), was soaked in this slurry and finally dried at ambient temperature.

2.4. Characterization

A Field-emission scanning electron microscopy (FESEM, Tescan MIRA 4|) was employed to characterize the surface morphology and the elemental analysis of the sample. A Thermo Scientific Nicolet IR100 (Madison, WI, USA) Fourier Transform Infrared (FT-IR) Spectroscopy was utilized to confirm the prepared compound. A Philips X'pert diffractometer (Cu Kα radiation) was employed to measure X-ray diffraction (PXRD).

2.5. Electrochemical measurements

The electrochemical behavior of the introduced flexible electrode was assayed by a three-electrode system in the presence of an electrolyte solution (3.0 M KOH). The working electrode was fabricated according to section (2.3). Ag/AgCl was employed as the reference electrode, and the Pt was utilized as a counter electrode. All electrochemical techniques, CV, GCD, and EIS, were recorded using a potentiostat/galvanostat device (PGSTAT-302 N, Eco Chemie, Netherlands). The following are some of the equations used to perform the necessary calculations:

The specific capacitance (C_{SP}) of the developed supercapacitor is estimated by Eq. (1) for CV measurement:

$$\mathbf{C_{SP}} = \frac{1}{\varvec{v}\,\mathbf{m}(\,\mathbf{V_2}-\mathbf{V_1})} \int_{\mathbf{V_1}}^{\mathbf{V_2}} \mathbf{I}\,(\mathbf{V})\,\mathbf{dV} \quad \text{Eq. (1)}$$

The specific capacitance value for supercapacitor electrodes in the charge-discharge plots was calculated by Eq. (2):

$$\mathbf{C_{sp}} = \frac{\mathbf{I}\varvec{\Delta}\,\mathbf{t}}{\mathbf{m}\varvec{\Delta}\,\mathbf{V}} \quad \text{Eq. (2)}$$

The specific energy density (E, Wh kg^{-1}) and power density (P, W kg^{-1}) values for a supercapacitor device are acquired by equations (3) and (4), respectively:

$E = ½\ C_{SP}\ (\Delta V)^2$ Equation. (3)

$P = E\ /\Delta t$ Equation. (4)

In these equations, v is the scan rate (V. s^{-1}), C_{SP} is the specific capacitance (F. g^{-1}), ΔV is the potential window (V), m is the mass of the electroactive material (g), I is the applied current (A), and Δt is the discharging time (s) [44–46].

3. Results and discussion

3.1. Morphology and structure

Figure 1A indicates the FESEM image for the synthesized TMU-12. The FESEM image of the TMU-12 at a 1 μm scale shows its surface morphology. TMU-12 has a uniform and almost hexagonal rod morphology. According to SEM images, the average size of TMU-12 is around

66 nm. EDX analysis (Fig. 1B) was employed for the elemental analysis or chemical characterization of the synthesized TMU-12. It shows that Co, O, C, and N elements are present in the fabricated compound. The FT-IR spectra for TMU-12 are illustrated in Fig. 1C. From this figure, it is evident that the recorded peaks for TMU-12 include the framework vibrations of the C-H bending of the benzene ring at 2750 cm^{-1} and 2850 cm^{-1}, the benzene ring at 1386 cm^{-1} and 1573 cm^{-1}, as well as the C = O absorption of the carboxylic acid group at 1615 cm^{-1} and the C-O stretching of the carboxylic acid group at 1380 cm^{-1}. These peaks well verify the existence of organic ligand functional groups in the TMU-12 compound. Figure 1D indicates the XRD pattern of the TMU-12. The experimental PXRD of the prepared TMU-12 is exactly comparable in pattern to the simulated one [43].

Insert Fig. 1

3.2. Electrochemical measurements of the prepared electrode

The electrochemical measurements of the electrode material were done in the presence of a 3.0 M KOH electrolyte. The CF (bare electrode) and TMU-12/CF electrodes were investigated in the potential range from 0.0 V to 0.35 V. The recorded voltammograms show that the TMU-12/CF has a larger CV area in comparison to the CF electrode, suggesting that the TMU-12/CF electrode has superior specific capacitance (Fig. 2A). The Nyquist plot drawn based on data obtained from electrochemical impedance spectroscopy (EIS) (Fig. 2B) indicates the impedance curve of the CF and TMU-12/CF. It can be seen that in the high frequency region in the Nyquist plot, the diameter of the semicircular curve for TMU-12/CF is less than that of CF, which indicates that TMU-12/CF has a lower charge transfer resistance (R_{CT}) and, as a result, has better conductivity [47]. It is also observed that in the high frequency region, the line slope is very steep, which indicates that the ion transport capacity is great. These results confirm that the proper pore structure enhances the ion transport capacity of the electrode and the capacitive behavior [48, 49]. These results demonstrate the appropriate performance of the TMU-12 as an electroactive material for electrode fabrication as a result of its special structure, which achieves an extensive range of electrochemically active sites for oxidation-reduction reactions and enhances electron-ion transport. The TMU-12/CF electrode is utilized as a work electrode (WE), and electrochemical experiments are carried out using the three-electrode system to examine the electrochemical behavior. The CV plots of the TMU-12/CF electrode were tested at varied scan rates from 0.005 $V.s^{-1}$ to 0.2 $V.s^{-1}$ in the presence of 3.0 M KOH electrolyte. As the scan rate increased from 0.005 $V.s^{-1}$ to 0.2 $V.s^{-1}$, no remarkable change in the voltammogram shape was seen, indicating that the TMU-12/CF electrode has good electrochemical reversibility and enhances mass transfer in electrolyte solution. The same shapes without obvious

change indicate good reversibility and acceptable rate capability (Fig. 2C). Voltammograms do not show observable redox peaks, and also at high scan rates, curves show a tilted shape. This reveals that the charge transports have a resistive behavior. The C_{SP} values were calculated using Eq. 1 for various applied scan rates. They are 206.93 F. g^{-1}, 112.603 F. g^{-1}, 101.902 F. g^{-1}, 98.2 F. g^{-1}, 85.74 F. g^{-1}, 75.2 F. g^{-1}, 66.96 F. g^{-1}, 60.43 F. g^{-1}, 41.91 F. g^{-1} for different applied scan rates from 0.005 V.s^{-1} to 0.2 V.s^{-1}, respectively. These amounts are presented in Fig. 2D and 2E. The highest C_{SP} value for TMU-12/CF electrode is 206.93 F. g^{-1} at = 0.005 V. s^{-1}. It can be clearly seen that the value of C_{SP} reduces with an increase in the scan rate. This phenomenon can be explained as follows: at lower scan rates, electrolyte ions have sufficient time to go through the available pores in the compound, resulting in a more efficient oxidation/reduction reaction and a higher capacitance [5]. Using potential scan rate data, the kinetics of charge storage can be investigated. Faradic or non-Faradic behavior of TMU-12/CF electrode can be examined by plotting the logarithm of the peak current (log i) versus the logarithm of the scan rate (log ()) according to this equation: (log i = b log () + log (a)). Where “a” and “b” are constants. Using the value of b (estimated from the slope of this graph), the charge-storage characteristics of the electrode material are determined. When b = 0.5, the process is a diffusion-controlled faradaic reaction; when b = 1, the process is capacitive. The b value for the TMU-12/CF electrode was obtained 0.44 (Fig. 2F), showing that the charge storage mechanism for the TMU-12/CF electrode is a diffusion-controlled process.

Insert Fig. 2

The electrochemical behavior of the introduced flexible electrode (TMU-12/CF) was further examined using the GCD method in 3.0 M KOH. GCD plots of the TMU-12/CF electrode at varied current densities, 6.0 A g^{-1} to 20 A g^{-1}, are observed in Fig. 3A. The GCD plots of the TMU-12/CF presents symmetrical shape, confirming the cceptable coulombic efficiency during the charge/discharge process (Fig. 3A). Based on the charge/discharge curves at different current densities, the C_{SP} values can be calculated by as shown in Fig. 3B, and 3C. TMU-12/CF exhibits a C_{SP} value of 53.31 F g^{-1} at 6.0 A g^{-1}. The specific capacitance plots manifest that TMU-12/CF indicates relatively good rate capability. Particularly, the specific capacitance value of

TMU-12/CF decreases from 53.31 F g^{-1} (at 6.0 A g^{-1}) to 23.41 F g^{-1} (at 20 A g^{-1}), and 56.09% of the initial specific capacitance value is maintained. It should be mentioned that TMU-12/CF shows excellent cycling stability after recording 2000 cycles in the presence of an aqueous electrolyte solution (KOH 3.0 M) at the scan rate of 0.04 V. s^{-1}. TMU-12/CF presents a specific capacitance value that was retained 90.85% after recording 2000 cycles (Fig. 3D). The stability of the TMU-12/CF electrodes even at a high scan rate makes it clearly an efficient choice for applications when fast charging is essential.

Insert Fig. 3

To examine the feasibility of using the prepared electrode, the symmetric supercapacitor devices were fabricated using the TMU-12/CF electrode in a 3.0 M KOH electrolyte. All recorded voltammograms at a

series of scan rates, 0005 V. s^{-1} – 0.1 V. s^{-1}, are indicated in Fig. 4A. It can be observed that the potential window has expanded to a wider range up to 1.6 V. The CV curves maintained their shape at higher scan rates, indicating that the prepared device has excellent rate capability, good reversibility, and proper electron transfer kinetics. Figure 4B and 4C indicate the amounts of calculated specific capacitances versus different scan rates. The highest specific capacitance amount for the assembled device was obtained 165.9 F. g^{-1} at an applied scan rate of 0.005 V. s^{-1}. The GCD curves at a series of current densities from 8.0 A g^{-1} to 10 A g^{-1} are nearly symmetric, showing high reversibility (Fig. 4D). It can be seen that with the increment of current density from 8.0 A g^{-1} to 10 A g^{-1}, the C_{SP} value of the introduced symmetric device reduces from 89.15 F g^{-1} to 55.37 F g^{-1}, exhibiting a rate capability of 61.01% (Fig. 4E, and 4F). This suggested system shows an energy density (E) of 7.93 Wh kg^{-1} along with a power density (P) of

3.2 kW kg^{-1}. These parameters are calculated using equations 1 and 2, respectively.

Insert Fig. 4

Table 1. Compares the supercapacitor electrode fabricated in this work with other works. This work indicates better specific capacitance value compared to some reported works based on Co-MOF, such as CoBDC (DMF), [Co_3 (2,6-NDC)$_3$(bipy)$_{1.5}$] and [Co(bpdc)(H_2O)$_2$]H_2O MOFs with capacitance value of 131.8 F g^{-1}, 147.3 F g^{-1} and 179.2 F g^{-1}, respectively at the scan rate of 0.01 V s^{-1} [50], Co-MOF/polyaniline-based electrode with electrochemical capacitance

Table 1
Comparison of supercapacitor electrode made based on cobalt MOF (TMU-12/CF) with other works.

Electrode	**Specific capacitance(F g^{-1})**	**Capacitance retention %**	**References**
CoBDC (DMF)	131.8 at 0.01 V s^{-1}	94.3% after 1000 cycles	[50]
$[Co_3$ (2,6-NDC)$_3$(bipy)$_{1.5}]$	147.3 at 0.01 V s^{-1}	95.8% after 1000 cycles	[50]
$[Co(bpdc)(H_2O)_2]$ H_2O	179.2 at 0.01 V s^{-1}	77.4% after 1000 cycles	[50]
Co-MOF/polyaniline	193 F g^{-1} at 0.01 V s^{-1}	82% after 3000 cycles	[51]
Co-MOF film	154.5 F g^{-1} at 0.01 V s^{-1}	98.5% after 1000 cycles	[39]
Co-MOF	980 F g^{-1} at 1 mA cm^{-2}	72.38% after 2000 cycles	[52]
Self-supported hierarchical Co-MOF	13.6 F cm^{-2} at 2 mA cm^{-2}	69.7% after 2000 cycles	[53]
Benzene-1,3,5-tricarboxylic acid-cobalt phosphate MOF (MOFCoP@rGO_2) hybrid electrode	133 F g^{-1} at 1 A g^{-1}	95% after 1000 cycles	[54]
Cobalt based inclined polycatenated MOF	446.8 F g^{-1} at 1.2 A g^{-1}	88.37% after 800 cycles	[55]
TMU-12/CF	206.93 F. g^{-1} at 0.005 V. s^{-1}	90.85% after 2000 cycles	**This work**

of 193 F g^{-1} at 0.01 V s^{-1} [51], and Co-MOF film with specific capacitance value of 154.5 F g^{-1} at 0.01 V s^{-1} [39]. This work has better stability compared to some Co MOF compounds, such as Co MOF with 72.38% capacitance retention after 2000 cycles [52], a self-supported hierarchical Co MOF with 69.7% retention after 2000 cycles [53], benzene-1,3,5-tricarboxylic acid-cobalt phosphate MOF hybrid electrode with 95% retention after 1000 cycles [54], a cobalt based inclined polycatenated with capacitance retention of 88.37% after 800 cycles [55] and a Co MOF film with 98.5% capacitance retention after 1000 cycles [39]. Therefore, the introduced TMU-12 MOF is an acceptable material to fabricate a flexible supercapacitor electrode with significant electrochemical properties.

Insert Table 1

4. Conclusions

MOFs are practical materials for supercapacitor electrodes due to their outstanding advantages, including 3D porous architecture, large surface area, and permeability to external elements, simple synthesis, and high-temperature resistance. Most studies on MOFs have been based on the utilization of synthetic materials involving a single linker and one metal. Nevertheless, the latest studies in this field have focused on the construction of novel MOFs using a similar metal with various oxidation states or two various metals or linkers, which lead to MOFs with higher catalytic activity than MOFs with a single linker or metal. This work is an excellent example of the performance of a mixed linker-synthesized MOF. In this work, the 3D porous MOF TMU-12 was used for the first time in the fabrication of a flexible supercapacitor electrode. The TMU-12/CF electrode was utilized as the working electrode, and different electrochemical techniques were performed to evaluate its electrochemical performance. The specific capacitance value for the TMU-12/CF electrode obtained CSP = 206.93 F. g^{-1} at = 0.005 V. s^{-1} in the presence of an aqueous electrolyte solution. The highest specific capacitance for the assembled device (symmetric supercapacitor) was obtained 165.9 F. g^{-1} at = 0.005 V. s^{-1} in a large potential window, 0.0 V–1.6 V. An E value of 7.93 Wh. kg^{-1} and a P value of 3.2 kW. kg^{-1} acquired for the supercapacitor device. According to the obtained results, MOFs are promising materials for constructing flexible supercapacitor electrodes owing to their unique properties and adjustable structures. Therefore, the synthesis and introduction of new MOFs are promising for the further development of supercapacitor electrode materials.

Declarations

Author contribution statement:

Hamideh Mohammadian-Sarcheshmeh, Mohammad Mazloum-Ardakani, and Meysam Safari: Conceived and designed the experiments; Performed the experiments; Analyzed and interpreted the data; Contributed reagents, materials, analysis tools or data; Wrote the paper.

Funding statement:

This work is based upon research funded by Iran National Science Foundation (INSF) under project No.4027759.

Competing interest statement:

The authors declare no conflict of interest.

Data availability:

All data generated or analyzed during this study are included in this published article.

Acknowledgements:

All authors listed have significantly contributed to the development and the writing of this article.

All authors are thankful for the financial support of the Research Council of Yazd University, Iran, for this research.

References

1. Shao, Y. *et al*. Design and mechanisms of asymmetric supercapacitors. *Chem. Rev.* **118**, 9233–9280 (2018). https://doi.org/10.1021/acs.chemrev.8b00252.
2. Han, X. *et al.* Construction of vacancies-enriched CuS/Fe_2O_3 with nano-heterojunctions as negative electrode for flexible solid-state supercapacitor. *J. Alloys Compd.* **916**,165443 (2022). https://doi.org/10.1016/j.jallcom.2022.165443.
3. Choudhary, N. *et al.* Asymmetric supercapacitor electrodes and devices, *Adv. Mater.* **29**, 1605336 (2017). https://doi.org/10.1002/adma.201605336.
4. Qi, D., Liu, Y., Liu, Z., Zhang, L., & Chen, X. Design of architectures and materials in in-plane micro-supercapacitors: current status and future challenges, *Adv. Mater.* **29**, 1602802 (2017). https://doi.org/10.1002/adma.201602802.
5. Chen, J. *et al.* MnO_2 grown in situ on graphene@ CNTs as electrode materials for supercapacitors. *Ceram. Int.* **41**, 12680–12685 (2015). https://doi.org/10.1016/j.ceramint.2015.06.099.
6. Zhou, P. *et al.* PVP derived nitrogen-doped porous carbon integrated with polyindole: nano/microspheres assembled by emulsion polymerization for asymmetric supercapacitors. *J. Mater. Chem A.* **10**, 10514–10524 (2022). https://doi.org/10.1039/D2TA00102K.
7. Mukhiya, T. *et al.* Designed assembly of porous cobalt oxide/carbon nanotentacles on electrospun hollow carbon nanofibers network for supercapacitor. *ACS Appl. Energy Mater.* **3**, 3435–3444 (2020). https://doi.org/10.1021/acsaem.9b02501.
8. Zong, S. *et al.* N-doped crumpled carbon nanotubes as advanced electrode material for supercapacitor. *J. Alloys Compd.* **928**, 167222 (2022). https://doi.org/10.1016/j.jallcom.2022.167222.
9. Mohanty, A. *et al.* An extensive review on three dimension architectural Metal-Organic Frameworks towards supercapacitor application. *J. Power Sources.* **488**,229444 (2021). https://doi.org/10.1016/j.jpowsour.2020.229444.
10. Yang, Y. *et al.* High-performance hybrid supercapacitor enabled by advantageous heterojunction boosted starfish-like ZnCo-S electrode. *J. Alloys Compd.* **928**,166997 (2022). https://doi.org/10.1016/j.jallcom.2022.166997.
11. Chen, Y. *et al.* MOF-derived Fe_2O_3 decorated with MnO_2 nanosheet arrays as anode for high energy density hybrid supercapacitor. *J. Chem. Eng.*, **417**,129243 (2021). https://doi.org/10.1016/j.cej.2021.129243.

12. Li, G. *et al.* Construction of Hierarchical NiCoO@ Ni-MOF Hybrid Arrays on Carbon Cloth as Superior Battery-Type Electrodes for Flexible Solid-State Hybrid Supercapacitors. *ACS Appl. Mater. Interfaces*., **11**,37675–37684 (2019). https://doi.org/10.1021/acsami.9b11994.
13. Shearer, G.C. *et al.* Tuned to perfection: ironing out the defects in metal–organic framework UiO-66. *Chem. Mat.* **26**,4068–4071 (2014). https://doi.org/10.1021/cm501859p.
14. Choi, K.M., Jeon, H.J., Kang, J.K., & Yaghi, O.M., Heterogeneity within order in crystals of a porous metal–organic framework. *J. Am. Chem. Soc.* **133**, 11920–11923 (2011). https://doi.org/10.1021/ja204818q.
15. Li, P. *et al.* Bottom-up construction of a superstructure in a porous uranium-organic crystal. *Science*. **356**, 624–627 (2017). 10.1126/science.aam7851.
16. Yan, Y. *et al.* Non-interpenetrated metal–organic frameworks based on Copper (II) paddlewheel and oligoparaxylene-isophthalate linkers: Synthesis, structure, and gas adsorption. *J. Am. Chem. Soc*. **138**,3371–3381 (2016). https://doi.org/10.1021/jacs.5b12312.
17. Y. Yang, *et al.* Rational construction of ternary ZnNiP arrayed structures derived from 2D MOFs for advanced hybrid supercapacitors and Zn batteries. *Electrochim. Acta*. **387**, 138548 (2021). https://doi.org/10.1016/j.electacta.2021.138548.
18. Cherusseri, J., Pandey, D., Kumar, K.S., Thomas, J., & Zhai, L., Flexible supercapacitor electrodes using metal–organic frameworks. *Nanoscale*. **12**, 17649–17662 (2020). https://doi.org/10.1039/D0NR03549A.
19. Chen, B. *et al.* High H_2 adsorption in a microporous metal–organic framework with open metal sites. *Angew. Chem*., **117**, 4823–4827 (2005). 10.1002/anie.200462787.
20. Zhou, S. *et al.* Cellulose nanofiber@ conductive metal–organic frameworks for high-performance flexible supercapacitors. *ACS Nano*. **13**, 9578–9586 (2019). https://doi.org/10.1021/acsnano.9b04670.
21. R. Wang, *et al.* Engineering metal organic framework derived 3D nanostructures for high performance hybrid supercapacitors. *J. Mater. Chem A*. **5**, 292–302 (2017). 10.1039/C6TA09143A.
22. Houshmand, S., Mazloum-Ardakani, M., Mohammadian-Sarcheshmeh, H., & Mohseni-Sardari, F., Highly Sensitive Non-Enzymatic Electrochemical Sensor to Detect an Important Neurotransmitter Using Cobalt-Based Metal-Organic Framework/Graphene Oxide Composite. *J. Electrochem. Soc*. **172**,017510 (2025). 10.1149/1945-7111/ada57e.
23. Mohseni-Sardari, *et al.* Enzyme-free glutamate sensor using peony flower-like structure of nickel metal–organic framework/MWCNTs nanocomposite. *Inorg. Chem. Commun*., **179**,114734 (2025). https://doi.org/10.1016/j.inoche.2025.114734.
24. Xia, H. *et al.* 2D MOF nanoflake-assembled spherical microstructures for enhanced supercapacitor and electrocatalysis performances. *Nano-Micro Lett*. **9**, 43 (2017). https://doi.org/10.1007/s40820-017-0144-6.
25. Saleem, M. *et al.* Exploring new frontiers in supercapacitor electrodes through MOF advancements. *J. Energy Storage*, **76**, 109822 (2024). https://doi.org/10.1016/j.est.2023.109822.

26. Sheberla, D., *et. al.* Conductive MOF electrodes for stable supercapacitors with high areal capacitance. *Nat. Mater*. **16**,220–224 (2017). https://doi.org/10.1038/nmat4766.
27. Salunkhe, R.R., *et. al.* Fabrication of symmetric supercapacitors based on MOF-derived nanoporous carbons. *J. Mater. Chem. A*,. **2**, 19848–19854 (2014). https://doi.org/10.1039/C4TA04277H.
28. Wang, Z., *et. al.* A porous Co $(OH)_2$ material derived from a MOF template and its superior energy storage performance for supercapacitors. *J. Mater. Chem. A*., **3**,20658–20663 (2015). https://doi.org/10.1039/C5TA04663G.
29. Xuan, W., Ramachandran, R., Zhao, C., Wang, F., Influence of synthesis temperature on cobalt metal-organic framework (Co-MOF) formation and its electrochemical performance towards supercapacitor electrodes. *J. Solid State Electrochem*. **22**, 3873–3881 (2018). https://doi.org/10.1007/s10008-018-4096-7.
30. You, B., Jiang, N., Sheng, M., & Sun, Y., Microwave vs. solvothermal synthesis of hollow cobalt sulfide nanoprisms for electrocatalytic hydrogen evolution and supercapacitors. *ChemComm*. **51**,4252–4255 (2015). https://doi.org/10.1039/C4CC09849H.
31. Worrall, S.D., *et. al.* Electrochemical deposition of zeolitic imidazolate framework electrode coatings for supercapacitor electrodes. *Electrochim. Acta*. **197**,228–240 (2016). https://doi.org/10.1016/j.electacta.2016.02.145.
32. Campagnol, N., *et. al.* Luminescent terbium-containing metal–organic framework films: new approaches for the electrochemical synthesis and application as detectors for explosives. *ChemComm*. **50**, 12545–12547 (2014). https://doi.org/10.1039/C4CC05742B.
33. Punde, N.S., *et. al.* Hybrid composite based on porous cobalt-benzenetricarboxylic acid metal organic framework and graphene nanosheets as high performance supercapacitor electrode. *ChemistrySelect*. **3**, 11368–11380 (2018). https://doi.org/10.1002/slct.201802721.
34. Klimakow, M., *et. al.* Mechanochemical synthesis of metal–organic frameworks: a fast and facile approach toward quantitative yields and high specific surface areas. *Chem. Mat*. **22**, 5216–5221 (2010). https://doi.org/10.1021/cm1012119.
35. Al-Ghoul, M., Issa, R., & Hmadeh, M., Synthesis, size and structural evolution of metal–organic framework-199 via a reaction–diffusion process at room temperature. *CrystEngComm*. **19**,608–612 (2017). https://doi.org/10.1039/C6CE02436J.
36. Ramachandran, R., *et. al.* Synthesis of copper benzene-1, 3, 5-tricarboxylate metal organic frameworks with mixed phases as the electrode material for supercapacitor applications. *Appl. Surf. Sci*. **460**, 33–39 (2018). https://doi.org/10.1016/j.apsusc.2017.11.271.
37. Khan, N.A., & Jhung, S.H. Synthesis of metal-organic frameworks (MOFs) with microwave or ultrasound: Rapid reaction, phase-selectivity, and size reduction. *Coord. Chem. Rev*. **285**,11–23 (2015). https://doi.org/10.1016/j.ccr.2014.10.008.
38. Díaz, R., *et. al.* J. Palma, Co8-MOF-5 as electrode for supercapacitors. *Mater. Lett*. **68**,126–128 (2012). https://doi.org/10.1016/j.matlet.2011.10.046.

39. Lee, D.Y. *et. al.* Unusual energy storage and charge retention in Co-based metal–organic-frameworks, *Micropor Mesopor Mater*. **153**, 163–165 (2012). https://doi.org/10.1016/j.micromeso.2011.12.040.
40. Yan, Y. *et. al.* Facile synthesis of vanadium metal-organic frameworks for high-performance supercapacitors. *Small*. **14**, 1801815 (2018). https://doi.org/10.1002/smll.201801815.
41. Campagnol, N., *et. al.* A hybrid supercapacitor based on porous carbon and the metal-organic framework MIL-100 (Fe). *ChemElectroChem*. **1**, 1182–1188 (2014). https://doi.org/10.1002/celc.201402022.
42. Bahiraee, Z., Fathi, S., & Safari, M., Facile synthesis of Fe_3O_4@ TMU-12 (Co-based magnetic MOF) for extraction of diazinon and chlorpyrifos from the environmental water samples. *Environ. Prog. Sustain*. **42**,e13971 (2023). https://doi.org/10.1002/ep.13971.
43. Masoomi, M.Y., Bagheri, M., & Morsali, A., Application of two cobalt-based metal–organic frameworks as oxidative desulfurization catalysts. *Inorg. Chem*. **54**, 11269–11275 (2015). https://doi.org/10.1021/acs.inorgchem.5b01850.
44. Mazloum-Ardakani, M., *et. al.* Fabrication of a high-performance hybrid supercapacitor using a modified graphene aerogel/cerium oxide nanoparticle composite, *J. Energy Storage*. **26**, 100998 (2019). https://doi.org/10.1016/j.est.2019.100998.
45. Mohammadian-Sarcheshmeh, H. & Mazloum-Ardakani, M., Porous carbohydrate–graphene aerogels synthesized by green method as electroactive supercapacitor materials. *Heliyon*. **10**, e29852 (2024). 10.1016/j.heliyon.2024.e29852.
46. Mohammadian-Sarcheshmeh, H., Mazloum-Ardakani, M., Ramazani, Z., & Abdollahi-Alibeik, M., Supercapacitor electrode based on graphene covalently functionalized with cross-linking inorganic-organic molecule. *Inorg. Chem. Commun*. **161**,111988 (2024). https://doi.org/10.1016/j.inoche.2023.111988.
47. Lv, Z. *et. al.* Honeycomb-lantern-inspired 3D stretchable supercapacitors with enhanced specific areal capacitance. *Adv. Mater*. **30**, 1805468 (2018). https://doi.org/10.1002/adma.201805468.
48. Cheng, Y. *et. al.* Flexible and cross-linked N-doped carbon nanofiber network for high performance freestanding supercapacitor electrode. *Nano Energy*. **15**, 66–74 (2015). https://doi.org/10.1016/j.nanoen.2015.04.007.
49. Kim, J.H., & Kim, B.-H., Hierarchical porous MnO_2/carbon nanofiber composites with hollow cores for high-performance supercapacitor electrodes: Effect of poly (methyl methacrylate) concentration, *Electrochim. Acta*. **200**, 174–181 (2016). https://doi.org/10.1016/j.electacta.2016.03.095.
50. Lee, D.Y. *et. al*. Supercapacitive property of metal–organic-frameworks with different pore dimensions and morphology. *Micropor. Mesopor. Mater*. **171**, 53–57 (2013). https://doi.org/10.1016/j.micromeso.2012.12.039.
51. Iqbal, M.Z. *et. al*. Co-MOF/polyaniline-based electrode material for high performance supercapattery devices. *Electrochim. Acta*. **346**, 136039 (2020). https://doi.org/10.1016/j.electacta.2020.136039.

52. Bhoite, A.A., Hubale, V.B., Sawant, V.A., & Tarwal, N.L., Cobalt-based metal–organic framework (Co-MOF) thin films with high capacitance for supercapacitor electrode. *J. Mater. Sci*. **59**,6807–6819 (2024). https://doi.org/10.1007/s10853-024-09591-8.
53. Zhu, G., *et. al.* A self-supported hierarchical Co-MOF as a supercapacitor electrode with ultrahigh areal capacitance and excellent rate performance. *ChemComm*. **54**, 10499-10502 (2018). https://doi.org/10.1039/C8CC03669A.
54. Vinoth Kumar, R., Vickraman, P., Arul Raja, T., & Ramya Bharathi, M.S., Cobalt phosphate-benzene-1, 3, 5-tricarboxylic acid metal–organic framework@ reduced graphene oxide electrodes for hybrid supercapacitors. *J. Mater. Sci*. **59**, 5498–5517 (2024). https://doi.org/10.1007/s10853-024-09525-4.
55. Rajak, R., Saraf, M., Mohammad, A., Mobin, S.M., Design and construction of a ferrocene based inclined polycatenated Co-MOF for supercapacitor and dye adsorption applications. *J. Mater. Chem. A*. **5**, 17998–18011 (2017). https://doi.org/10.1039/C7TA03773B.

Figures

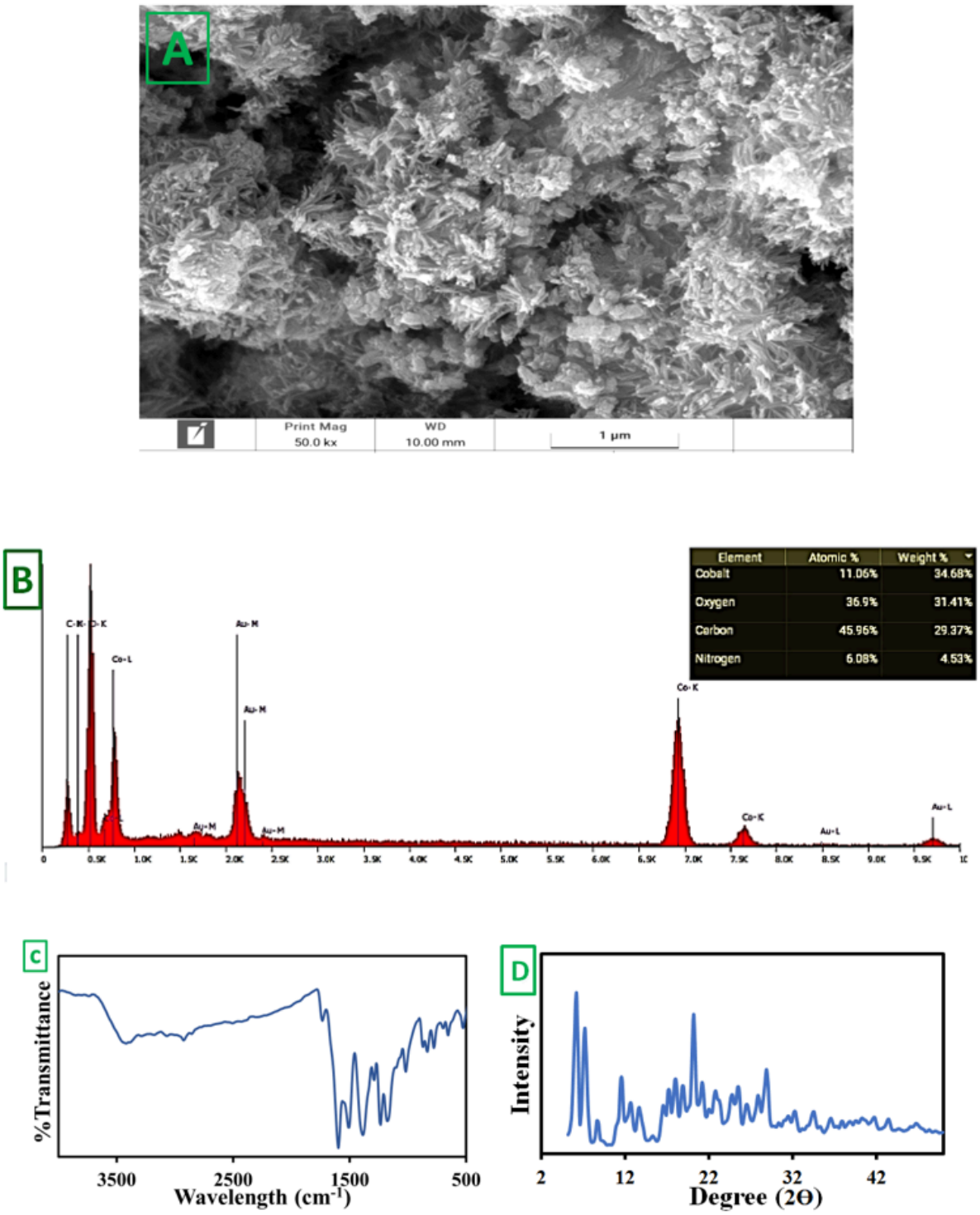


Figure 1

(A) FESEM analysis, (B) EDX analysis, (C) FT-IR results, and (D) XRD patterns for TMU-12 MOF.

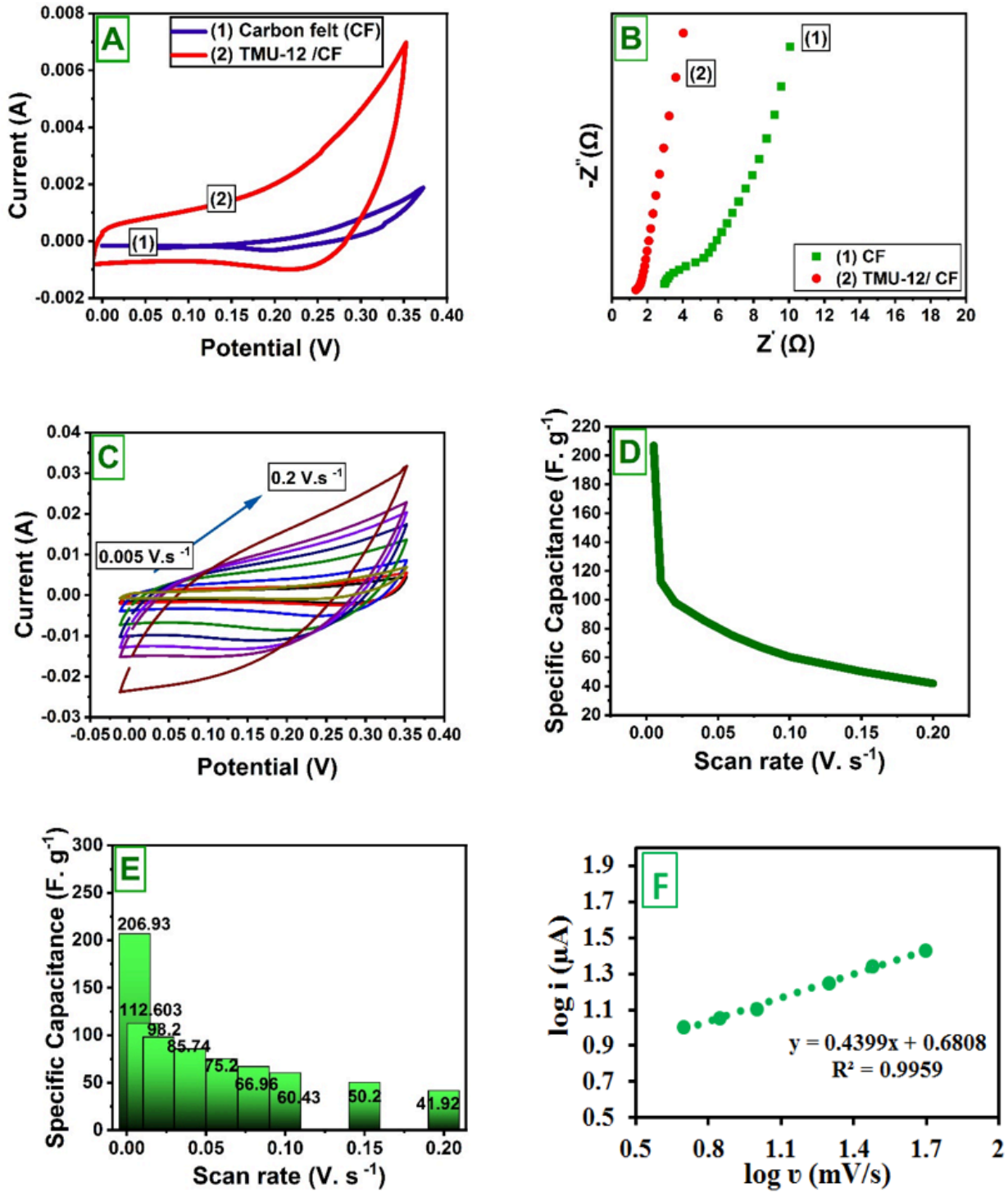


Figure 2

(A) Compare the electrochemical behavior of electrodes, (1) CF, and (2) TMU-12/CF in KOH electrolyte (3.0 M) at the potential region 0.0 V to 0.35 V. (B) Comparing Nyquist plot for (1) CF, and (2) TMU-12/CF. (C) Cyclic voltammograms at various scan rates from 0.005 $V.s^{-1}$ to 0.2 $V.s^{-1}$, (D) plot of calculated C_{SP} versus different scan rates, (E) the calculated C_{SP} for different scan rates. (F) Investigation of charge-storage characteristic for TMU-12/CF electrode.

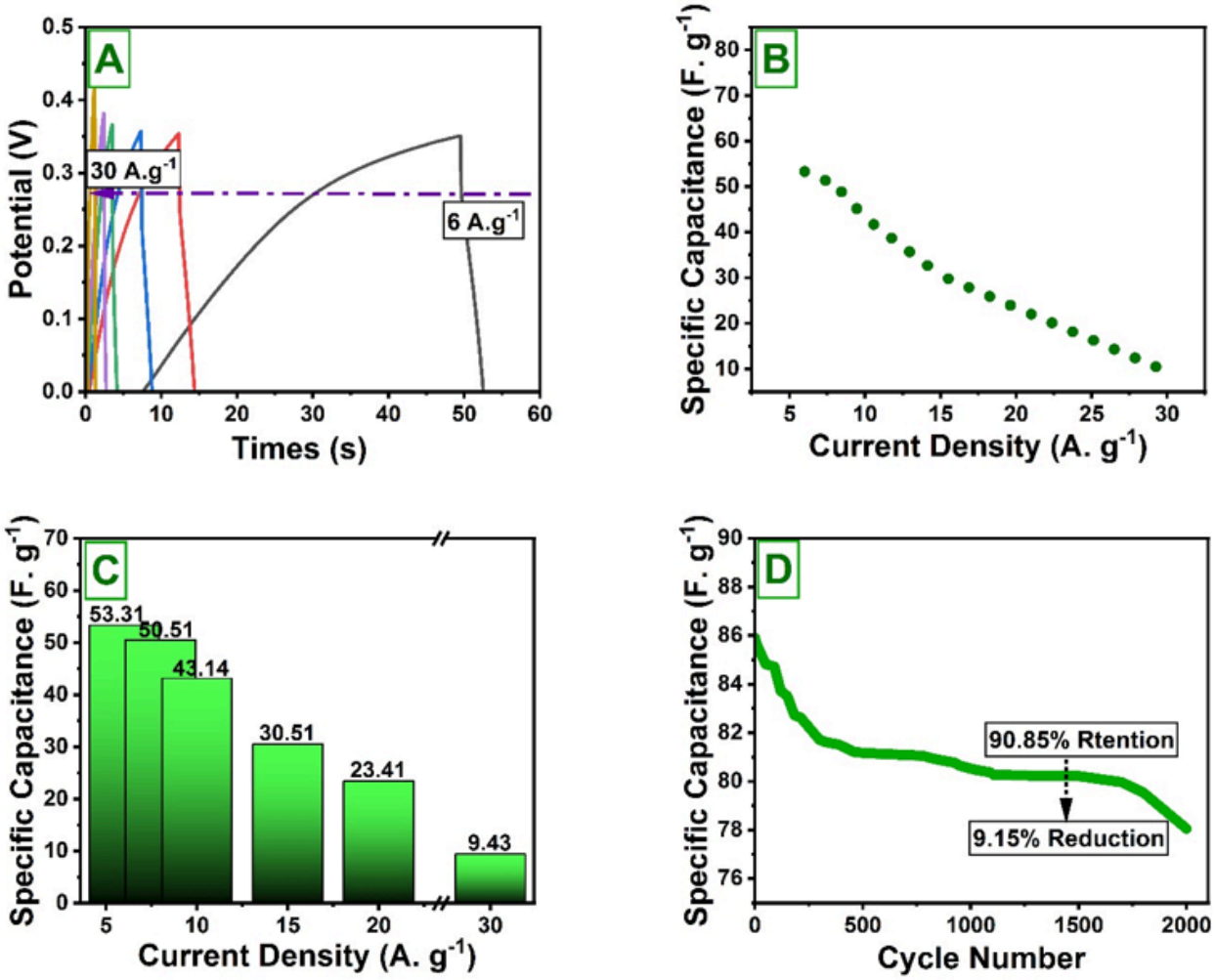


Figure 3

(A) GCD curves in various current densities for TMU-12/CF in KOH electrolyte (3.0 M) at the potential region 0.0 V to 0.35 V, and (B) plot of calculated C_{SP} versus current densities. (C) The calculated C_{SP} in various current densities. (D) Investigation of stability for TMU-12/CF electrode in KOH electrolyte (3.0 M) at scan rate of 0.04 V. s^{-1}.

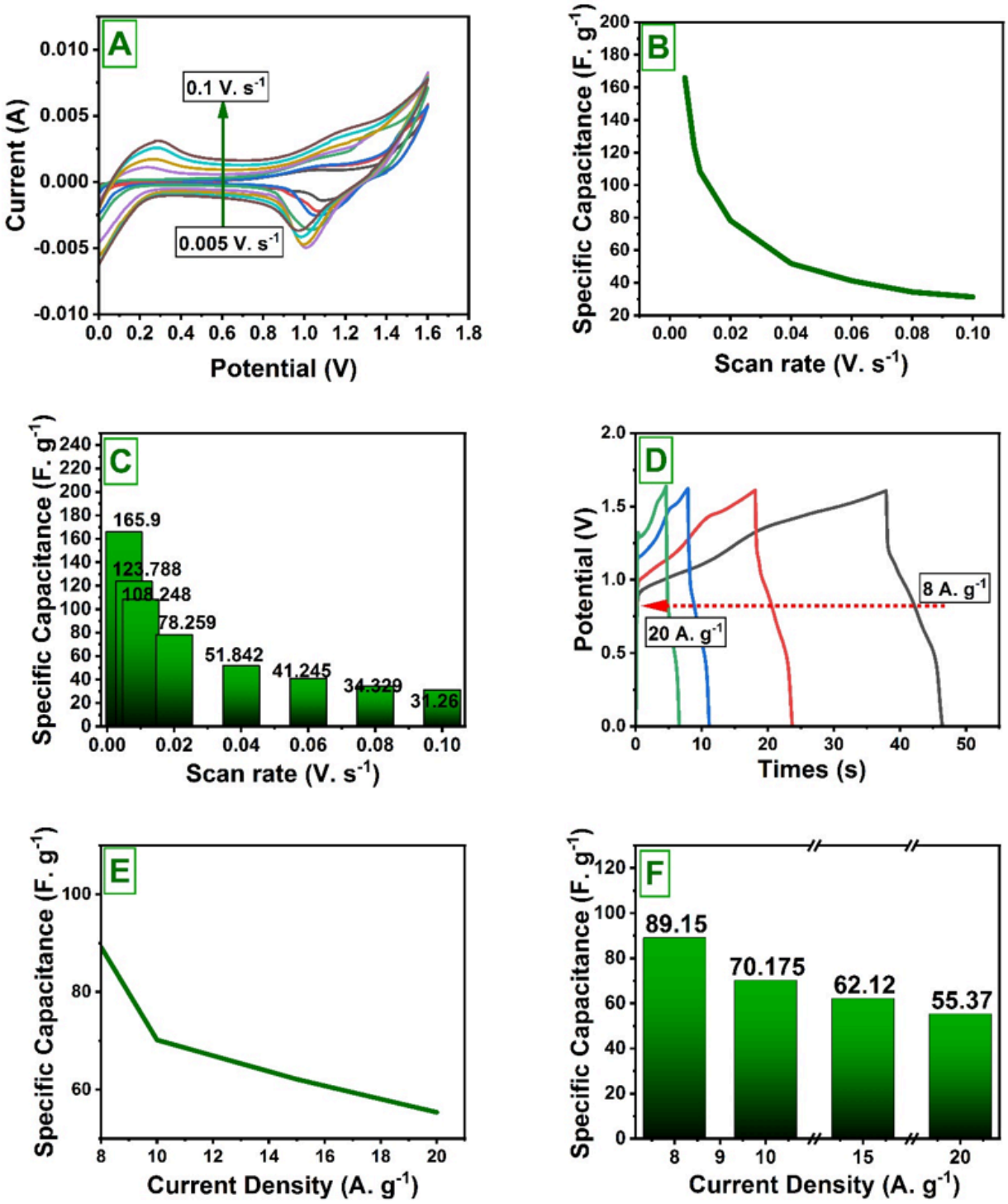


Figure 4

Examination of the electrochemical behavior (two-electrode system) for TMU-12/CF electrode, in KOH electrolyte (3.0 M) at the potential region 0.0 V to 1.6 V: (A) Cyclic voltammograms at different scan rates from 0.005 $V.s^{-1}$ to 0.1 $V.s^{-1}$, (B) plot of calculated C_{SP} versus different scan rates, (C) the calculated C_{SP} amount for different scan rates, (D) GCD curves in various current densities from 8.0 A g^{-1} to 30 A g^{-1}, and (E) plot of calculated C_{SP} versus the applied current densities, (F) the calculated C_{SP} for various current densities.